

# Origin of Selective Production of Hydrogen Peroxide by Electrochemical Oxygen Reduction

Xunhua Zhao and Yuanyue Liu\*



Cite This: *J. Am. Chem. Soc.* 2021, 143, 9423–9428



Read Online

ACCESS |

Metrics & More

Article Recommendations

Supporting Information

**ABSTRACT:** Oxygen reduction reaction (ORR) is one of the most important electrochemical reactions. Starting from a common reaction intermediate  $^*-\text{O}-\text{OH}$ , the ORR splits into two pathways, either producing hydrogen peroxide ( $\text{H}_2\text{O}_2$ ) by breaking the  $^*-\text{O}$  bond or leading to water formation by breaking the  $\text{O}-\text{OH}$  bond. However, it is puzzling why many catalysts, despite the strong thermodynamic preference for the  $\text{O}-\text{OH}$  breaking, exhibit high selectivity for hydrogen peroxide. Moreover, the selectivity is dependent on the potential and pH, which remain not understood. Here we develop an advanced first-principles model for effective calculation of the electrochemical reaction kinetics at the solid–water interface, which were not accessible by conventional models. Using this model to study representative catalysts for  $\text{H}_2\text{O}_2$  production, we find that breaking the  $\text{O}-\text{OH}$  bond can have a higher energy barrier than breaking  $^*-\text{O}$ , due to the rigidity of the  $\text{O}-\text{OH}$  bond. Importantly, we reveal that the selectivity dependence on potential and pH is rooted into the proton affinity to the former/later O in  $^*-\text{O}-\text{OH}$ . For single cobalt atom catalyst, decreasing potential promotes proton adsorption to the former O, thereby increasing the  $\text{H}_2\text{O}_2$  selectivity. In contrast, for the carbon catalyst, the proton prefers the latter O, resulting in a lower  $\text{H}_2\text{O}_2$  selectivity in acid condition. These findings explain the experiments and highlight the kinetic origins of the selectivity. Our work improves the understanding of ORR by uncovering the proton affinity as a new factor and provides a new model to effectively simulate the atomic-level kinetics of heterogeneous electrochemistry.

## INTRODUCTION

Oxygen reduction reaction (ORR)<sup>1,2</sup> is one of the most important electrochemical reactions and lies at the center of various techniques to address the energy and environmental issues. It can convert  $\text{O}_2$  to  $\text{H}_2\text{O}$  by  $\text{O}_2 + 4\text{H}^+ + 4\text{e}^- \rightarrow 2\text{H}_2\text{O}$  (4e pathway) or to  $\text{H}_2\text{O}_2$  by  $\text{O}_2 + 2\text{H}^+ + 2\text{e}^- \rightarrow \text{H}_2\text{O}_2$  (2e pathway). The 4e pathway is critical to the fuel cell<sup>3</sup> that converts fuels to electricity and can be used in many applications such as transportation. The 2e pathway, which receives great interest recently, provides an efficient and decentralized way to produce  $\text{H}_2\text{O}_2$ , which has various applications<sup>4–6</sup> including water disinfection, bleaching, and energy carrier. These two pathways split after forming the  $^*-\text{O}-\text{OH}$  intermediate (where  $^*$  denotes an active site of the catalyst, and  $-$  emphasizes the key bonds). The breaking of the  $^*-\text{O}$  bond will produce  $\text{H}_2\text{O}_2$ , while the breaking of the  $\text{O}-\text{OH}$  bond will lead to  $\text{H}_2\text{O}$  formation. Therefore, it is important to understand the bond breakings of  $^*-\text{O}-\text{OH}$  for selective production.

The thermodynamics of the bond breakings have been extensively studied on a wide range of catalysts. Interestingly, the  $\text{O}-\text{OH}$  breaking is always thermodynamically much more favorable than the  $^*-\text{O}$  breaking, including the catalysts that have a moderate/high selectivity for  $\text{H}_2\text{O}_2$  production. For example, the catalyst of single cobalt atom embedded in nitrogen doped graphene (Co–N–C)<sup>7,8</sup> has a  $\text{H}_2\text{O}_2$  selectivity

ranging from 60% to 90%, while the density functional theory (DFT) calculations show that the breaking of  $\text{O}-\text{OH}$  is thermodynamically more favorable than breaking of  $^*-\text{O}$  by  $\sim 0.5$  eV.<sup>8</sup> Similarly, the Pd/Au alloy<sup>9</sup> has  $\text{H}_2\text{O}_2$  selectivity up to 95%, while the DFT results indicate that  $\text{O}-\text{OH}$  is easier to break than  $^*-\text{O}$  in thermodynamics by 0.30 eV. In addition, the selectivity is affected by the potential and pH. For example, when decreasing the potential  $V_{\text{RHE}}$  (potential relative to reversible hydrogen electrode, RHE) from 0.5 to 0.1 V, the  $\text{H}_2\text{O}_2$  selectivity of Co–N–C in acid condition increases from 60% to 80%.<sup>7</sup> For carbon materials (without metal), the acid condition typically results in a lower  $\text{H}_2\text{O}_2$  selectivity (18–82%)<sup>10</sup> than the alkaline condition (>92%).<sup>11,12</sup> The apparent contradiction between thermodynamics and the experiments, as well as the potential and pH dependence, calls for better understanding of the mechanism underlying the selectivity.

In this work, we develop an advanced first-principles model to access the kinetic information on the electrochemical steps

Received: February 25, 2021

Published: June 16, 2021



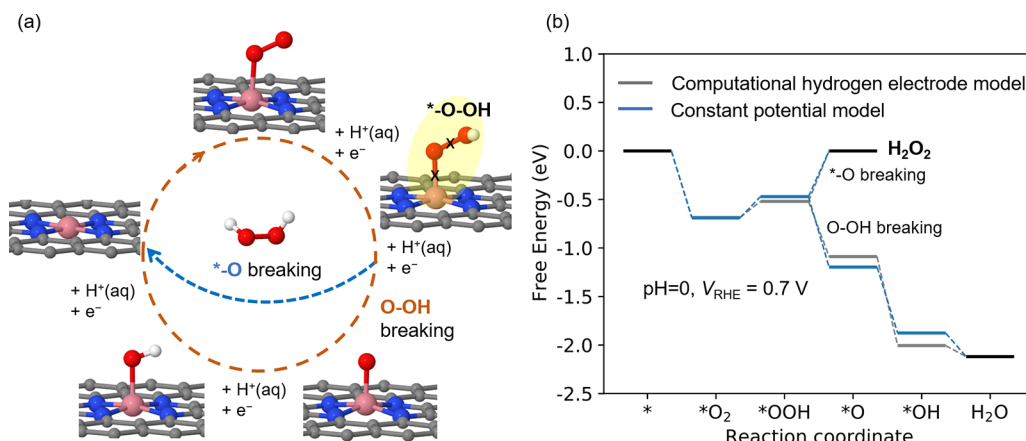


**Figure 1.** (a) Pathways of ORR illustrated on a single cobalt atom embedded in nitrogen doped graphene (Co–N–C). They split after \*–O–OH (highlighted) through \*–O breaking or O–OH breaking: Co, pink; C, gray; O, red; H, white. (b) Free energy diagrams of the ORR on Co–N–C, calculated using different models, both indicating a strong thermodynamic preference for the O–OH breaking.

at the solid–water interface, which cannot be accessed using conventional models. We find that the activation energy of O–OH breaking can be higher than that of \*–O breaking, and they show significantly different electron transfer behavior. Moreover, we find the potential and pH dependences are both reflected in the behavior of the proton, whose preference and affinity to the two O in \*–O–OH are tuned by the potential and pH. Our work offers new fundamental insights into the selectivity mechanism of ORR, highlights the kinetic factors that are missing in the conventional first-principles models for heterogeneous electrochemistry, and provides an effective tool capturing these factors to uncover the atomic-level kinetics.

## METHODS

The conventional first-principles methods for modeling electrochemistry at the solid–water interface, such as the computational hydrogen electrode model (CHEM),<sup>13</sup> often neglect or oversimplify the complexities including the following. (1) The elementary steps of the electrochemical reaction typically occur at constant electrode potential.<sup>14–22</sup> Consequently, the system often has net electronic charges changing along the reaction coordinate.<sup>18,21</sup> These charges on the surface can significantly change the chemical activity of the solid.<sup>23–25</sup> However, conventional models<sup>2,7,8,13,26–28</sup> often assume the system has zero (or constant) net electronic charges and neglect the surface charge effect. (2) The liquid water has numerous configurations with different interactions with the reaction species, and these configurations/interactions can also evolve along the reaction coordinate. However, conventional models often neglect the atomic structure of water by assuming it is a continuous medium (i.e., implicit solvent), or they consider only limited configurations with one or few water molecules.<sup>29,30</sup> This neglect/oversimplification is problematic especially for reactions producing polar species, which form dynamic hydrogen bonding network with explicit water molecules.<sup>23,31</sup> (3) To make things more complicated, the water configuration and the net electronic charges are coupled with each other, both fluctuating and evolving along the reaction coordinate. The conventional models thus fail to describe the kinetics of electrochemistry at the solid–water interface; instead, they are often employed to calculate the thermodynamics (i.e., the energy difference between the products and the reactants) of individual steps, which are then used to evaluate the catalyst performance.

To overcome these limitations, here we develop a “constant-potential hybrid-solvation dynamic model” (CP-HS-DM). This model uses several layers of explicit water molecules<sup>32,33</sup> in conjunction with implicit solution<sup>34,35</sup> to solvate the reaction species. The electrons are coupled with a fictitious potentiostat<sup>19</sup> so that the Fermi level of the system fluctuates around a constant and the number of electrons

evolves following the grand-canonical distribution at the preset electrode potential. The net electronic charges are balanced by the ionic charges in the implicit solution, keeping the system charge neutral. The constrained ab initio molecular dynamics (AIMD) simulations are performed with reaction coordinate gradually changing from the initial to the final state (“slow-growth” approach<sup>36,37</sup>). For each value of the reaction coordinate, we extract the corresponding mean force<sup>38</sup> acting on the reaction coordinate. The integration of the mean force with respect to the reaction coordinate will yield the free energy profile, from which the activation energy can be identified. The key feature of the CP-HS-DM is the implementation of the constant-potential condition for electrons to the slow-growth AIMD, which enables the evaluation of the kinetics of heterogeneous electrochemistry. More details can be found in the Supporting Information.

## RESULTS AND DISCUSSION

Figure 1a shows the general schematic of the ORR process under acid condition on Co–N–C as an example: starting from a common reaction intermediate \*–O–OH, the ORR splits in the pathway: (1) if \*–O bond is broken, then H<sub>2</sub>O<sub>2</sub> will form in solution, leaving a bare substrate (2e pathway); (2) if O–OH bond is broken, then H<sub>2</sub>O will form in solution, leaving an \*O that can be further hydrogenated to H<sub>2</sub>O (4e pathway). As mentioned in the Introduction section, previous DFT calculations<sup>8</sup> based on CHEM indicate that breaking the O–OH bond to form \*O is much more thermodynamically favorable than breaking the \*–O bond. This apparently contradicts the experimental observation that the H<sub>2</sub>O<sub>2</sub> formation is preferred.<sup>7,8</sup> Considering that CHEM may not be accurate as it neglects the surface charge and its evolution during the reaction<sup>30,39</sup> as discussed in the Methods section, we re-evaluate the thermodynamics using the constant-potential (CP) method (see Supporting Information for details), where the number of electrons in the system is tuned to match the Fermi level to the electrode potential. As shown in Figure 1b and Figure S2, the free energies of the intermediates calculated using CP model are more or less similar to those obtained from CHEM and confirm the strong thermodynamic preference for the O–OH bond breaking and the H<sub>2</sub>O formation (for example, at V<sub>RHE</sub> = 0.7 V, breaking O–OH is thermodynamically more favorable than \*–O by 1.2 eV). The apparent contradiction between thermodynamics and the experiments is common for H<sub>2</sub>O<sub>2</sub> production catalyst (see Figure S5 for a different catalyst, Pd/Au alloy) and drives us to

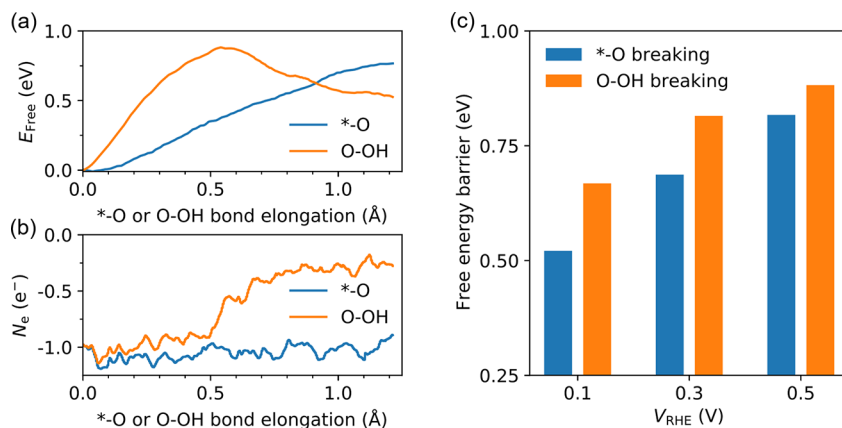


**Figure 2.** Free energy profile (a) and net electron evolution (b) during the bond breakings under  $V_{\text{RHE}} = 0.5$  V. (c) Activation energies for  $^*-\text{O}$  and  $\text{O}-\text{OH}$  breakings under different potentials. These kinetics are calculated using CP-HS-DM.

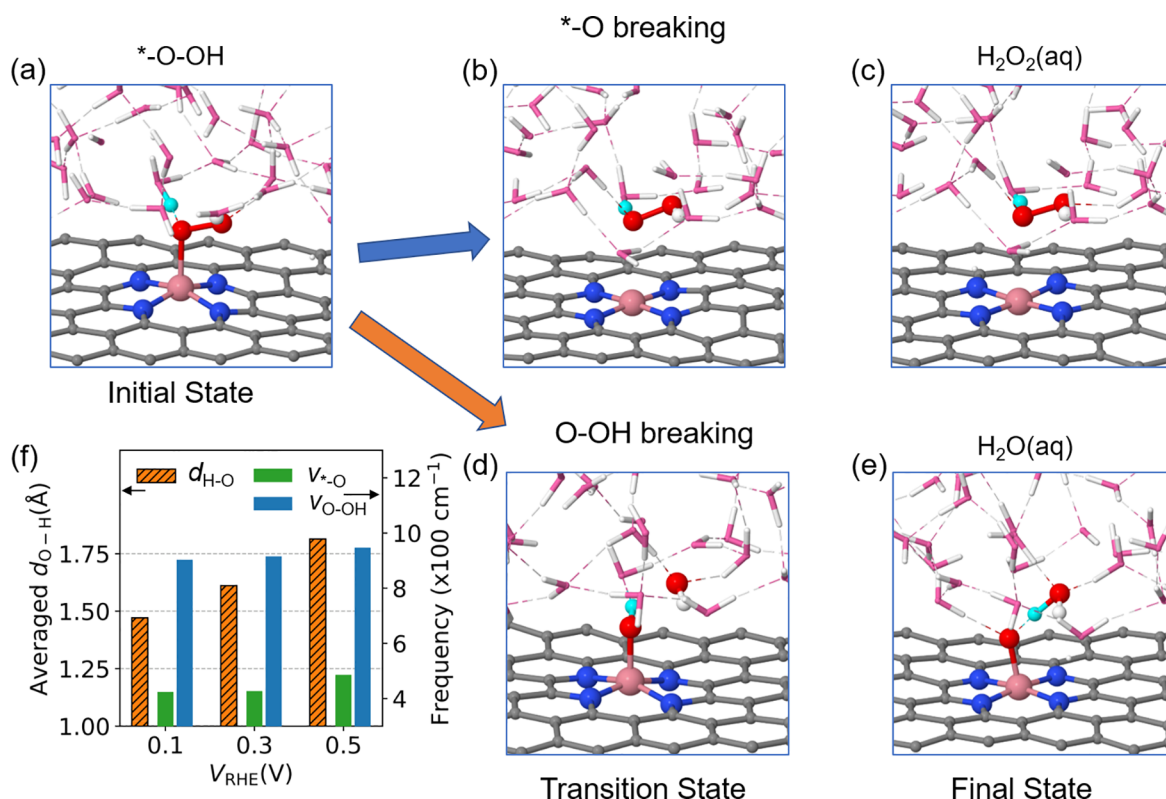


**Figure 3.** Atomic structure evolutions for the  $^*-\text{O}$  bond breaking (a  $\rightarrow$  b  $\rightarrow$  c) and  $\text{O}-\text{OH}$  bond breaking (a  $\rightarrow$  d  $\rightarrow$  e) under  $V_{\text{RHE}} = 0.3$  V: Co, pink; C, gray; O, red; H, white; proton, cyan. (f) The average length of the hydrogen bond of the former O in  $^*-\text{O}-\text{OH}$  at the initial state is presented by the orange bar with stripes (left-side y axes), while the vibrational frequencies of  $^*-\text{O}$  and  $\text{O}-\text{OH}$  bonds are shown as green and blue bars (right-side y axes).

investigate the kinetics especially the activation energies of the  $^*-\text{O}$  and  $\text{O}-\text{OH}$  bond breakings.

Then we calculate the energy barriers of the  $^*-\text{O}$  and  $\text{O}-\text{OH}$  bond breakings using the CP-HS-DM. As shown in Figure 2b, for Co-N-C, indeed the  $^*-\text{O}$  breaking has a lower barrier than the  $\text{O}-\text{OH}$  breaking. This agrees with experiments and indicates the kinetic origin of the selectivity. By examining the evolution of the free energy and the number of electrons during the bond breaking process, we find the  $^*-\text{O}$  and  $\text{O}-\text{OH}$  bond breakings have significantly different kinetic behaviors. These are shown in Figure 2a, using  $V_{\text{RHE}} = 0.5$  V as an example. For the  $\text{O}-\text{OH}$  bond breaking, the stretching of the  $\text{O}-\text{OH}$  bond increases the free energy up to a stage where

the system abruptly gains the electron to ionize the OH; after that, the free energy drops due to the solvation of the ionized OH. In contrast, during the  $^*-\text{O}$  breaking, the free energy increases and then starts to saturate while the number of electrons remain nearly unchanged, implying that the OOH is already ionized at the initial state before detachment from the catalyst. Note that even within the limited range of the bond length elongation considered here, the final state of  $\text{O}-\text{OH}$  bond breaking is already lower in energy than that of  $^*-\text{O}$  bond breaking, which is consistent with the thermodynamic preference as indicated by other models. These results suggest that the initial stretching of the  $\text{O}-\text{OH}$  bond can build up an energy barrier larger than that for breaking  $^*-\text{O}$  bond. We also

calculate the activation energies of bond breakings for a different catalyst, Pd/Au alloy,<sup>9</sup> and find that the activation energy of  $^*-\text{O}$  breaking is also lower than that of O–OH breaking (Figure S5), similar to the Co–N–C case and consistent with the experiments.<sup>9</sup> This suggests that the kinetic origin of the  $\text{H}_2\text{O}_2$  selectivity is a universal phenomenon.

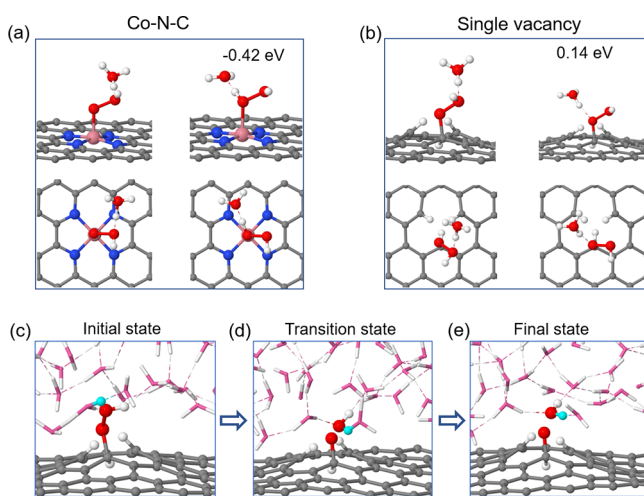
It is worth noting that although the free energy profile of  $^*-\text{O}$  breaking on Co–N–C seems to reach a plateau within the range of the bond length elongation ( $<3$  Å) considered in Figure 2a, it may drop at larger  $^*-\text{O}$  distances due to the enhanced solvation of the product ( $\text{H}_2\text{O}_2$ ) and the entropy.<sup>40</sup> However, calculating the free energy at such distances is computationally very expensive for AIMD, as it requires more water molecules and longer MD time to sample the phase space. Thus, we are not able to obtain the free energy profile beyond the distance range in Figure 2a. Another thing worth noting is that the Co–N–C carries positive electronic charge (Figure 2b). This is because the applied electrode potential (0.5 V vs RHE) in Figure 2b is higher than the potential of zero charge of Co–N–C ( $-0.42$  V vs RHE). Thus, when the Co–N–C is charged to the desired electrode potential, it will lose electrons.

Figure 2b also shows that decreasing the potential lowers the energy barriers of bond breakings. This is well expected because decreasing the potential increases the electron energy and thus facilitates the electrochemical reduction reaction. Interestingly, our results for acid conditions show that decreasing the potential leads to a larger difference in the energy barrier between  $^*-\text{O}$  and O–OH breakings for the Co–N–C, thereby increasing the selectivity for the  $\text{H}_2\text{O}_2$  formation. This is consistent with the experiments. To understand the origin of the potential dependent selectivity, we examine the atomic structure evolutions during the bond breaking processes. These are shown in Figure 3 using  $V_{\text{RHE}} = 0.3$  V as an example. We find that at the initial state, the proton prefers to be close to the former O in  $^*-\text{O}-\text{OH}$  species, i.e., the O bonded to the site. This preference is seen not only in AIMD simulations but also in a simple “static” model (Figure 4a), where one  $\text{H}_3\text{O}^+$  is used as a probe and its binding with the former O is stronger than the latter O by 0.42 eV. When

the  $^*-\text{O}$  is broken, the proton will attach to the OOH forming  $\text{H}_2\text{O}_2$  in solution (Figure 3b,c). Alternatively, when the O–OH is broken, the proton will attach to the O left on the substrate, forming  $^*\text{OH}$  on the substrate and  $\text{OH}^-$  in solution (then the H in  $^*\text{OH}$  will combine with  $\text{OH}^-$  to form  $\text{H}_2\text{O}$ , leaving  $^*-\text{O}$  on the substrate) (Figure 3d,e). When the potential decreases, the proton gets closer to the former O, as indicated by their average distance (Figure 3f) computed from the constant-potential AIMD simulations of the initial state (Figure S3), suggesting a stronger binding. As this distance gets shorter, the  $^*-\text{O}$  bond length gets longer while the O–OH is less affected (see Figure S4). Consistent with the bond length changes, the vibration frequencies of  $^*-\text{O}$  and O–OH decrease, with  $^*-\text{O}$  being more significant (see Figure 3f). Consequently, the energy barrier for breaking  $^*-\text{O}$  is more significantly lowered than that for O–OH, which increases the selectivity of  $\text{H}_2\text{O}_2$  production. These results highlight the role of proton affinity in the selectivity, which is not shown before.

The proton affinity also explains the pH dependence observed for the carbon catalyst.<sup>10,11</sup> It is known that the activity of the carbon catalyst comes from the defects.<sup>10</sup> One of the most common defects is the single vacancy in graphitic C, as shown in Figure 4b, where the three C atoms near the vacancy are passivated by H. These H are very stable, with the passivation energies of  $-1.70$  eV,  $-0.82$  eV, and  $-1.36$  eV, respectively, at  $V_{\text{RHE}} = 0.7$  V (see Supporting Information for the details). The OOH can form on one of these three C atoms. Different from the Co–N–C where the proton favors the former O in  $^*-\text{O}-\text{OH}$ , the C single vacancy site has the latter O preferred by the proton. This is seen in both the static model (Figure 4b) and the AIMD simulations. Due to the proximity, the proton can immediately stabilize the OH anion once it is formed from the breaking of the O–OH bond and thus facilitate its breaking. Indeed, our simulation of the O–OH breaking process using the CP-FS-DM confirms that the stabilization of the OH anion is by proton forming  $\text{H}_2\text{O}$  (Figure 4c,e). Compared with the system without proton (mimicking the pH neutral or alkaline condition), the energy barrier of O–OH breaking reduces by 0.14 eV when the proton is added, while the energy barrier of  $^*-\text{O}$  breaking does not change. This explains why the acid condition gives a lower selectivity for  $\text{H}_2\text{O}_2$  formation on carbon catalyst.

Why does the proton prefer the former O for Co–N–C catalyst while latter O for carbon? This is due to the steric effect of the hydrogen atoms passivating the C atoms near the active site, which hinders the proton from approaching the former O adsorbed on the site. As shown in Figure 4b, there are two H at the same side of graphene as OOH, with the distances to the former O being 1.86 and 1.94 Å. Such short distances are partially due to the short C–O bond length (1.52 Å, much shorter than the Co–O length: 1.88 Å). As a result, the former O is closely attached to the catalyst surface, and any other adsorbates nearby could hinder its accessibility by proton. To confirm the hindering effect, we remove the two H atoms at the same side as OOH and recalculate the binding energy of the proton to the former and latter O. Indeed, without them, the proton prefers the former O by 0.50 eV, which is the same as the Co–N–C case. One may wonder if in reality these two H can be at the other side of graphene opposite to OOH so that the hindering effect would be minimized or not exist. To test this possibility, we intentionally relocate one or two H to the other side and find that the structure evolves back to the original structure, due to the



**Figure 4.** Atomic structures of  $\text{H}_3\text{O}^+$  bonded with different O in  $^*-\text{O}-\text{OH}$  on Co–N–C (a) and single vacancy defect in graphene (b). The numbers show the relative binding energy. (c–e) Structure evolution of the O–OH breaking on single vacancy defect.

repelling by the third H adsorbed on the other side of the site. Considering the universally short C–O bond length regardless of the exact atomic structure of the site, we anticipate that the sites near the adsorbates would generally have lower selectivity for  $H_2O_2$  production under acid condition due to the difficulty in accessing the former O of OOH by proton.

## CONCLUSION

In summary, we developed a “constant-potential hybrid-solvation dynamic model” (CP-HS-DM) for first-principles simulations of the electrochemical kinetics at the solid–water interface. By applying this model, we uncovered the origin of the selective  $H_2O_2$  production by oxygen reduction reaction, as well as the potential and pH dependence, which were elusive previously. Specifically, we found that the initial stretching of the O–OH bond can induce an energy barrier higher than the breaking of  $^*O$ , thus preferring the  $H_2O_2$  formation. Moreover, we find that the proton affinity plays a critical role in the selectivity. For the single cobalt atom catalyst, decreasing potential promotes proton adsorption to the former O in  $^*O-OH$ , thereby increasing the  $H_2O_2$  selectivity. In contrast, for the carbon catalyst, the proton prefers the latter O, resulting in a lower  $H_2O_2$  selectivity in acid condition. Our work offers new insights into the ORR selectivity and provides a new model to effectively simulate the atomic-level kinetics of electrochemistry at the solid–water interface.

## ASSOCIATED CONTENT

### Supporting Information

The Supporting Information is available free of charge at <https://pubs.acs.org/doi/10.1021/jacs.1c02186>.

Details about the CP-HS-DM, H passivation energy for carbon catalyst, dependence on the first-principles method, pH setting, details of the bond lengths and vibration frequencies, thermodynamics and kinetics of ORR on Pd/Au, other H-electron transfer steps, comparison with the barriers calculated using a charge-neutral static model, effect of water on the other side of graphene, and electronic factors affecting the proton affinity (PDF)

## AUTHOR INFORMATION

### Corresponding Author

**Yuanyue Liu** – *Texas Materials Institute, The University of Texas at Austin, Austin, Texas 78712, United States*  
ORCID: [0000-0002-5880-8649](https://orcid.org/0000-0002-5880-8649); Email: [yuanyue.liu@austin.utexas.edu](mailto:yuanyue.liu@austin.utexas.edu)

### Author

**Xunhua Zhao** – *Texas Materials Institute, The University of Texas at Austin, Austin, Texas 78712, United States*

Complete contact information is available at:  
<https://pubs.acs.org/10.1021/jacs.1c02186>

### Notes

The authors declare no competing financial interest.

## ACKNOWLEDGMENTS

This work is supported by the NSF (1900039 and 2029442), the Welch Foundation (F-1959-20180324), ACS PRF (60934-DNI6), and DOE (DE-EE0007651). This work used computational resources at National Renewable Energy Lab, the

Extreme Science and Engineering Discovery Environment (XSEDE) through allocation TG-CHE190065, the Center for Nanoscale Materials at Argonne National Lab, and the Center for Functional Nanomaterials at Brookhaven National Laboratory.

## REFERENCES

- (1) Chu, S.; Cui, Y.; Liu, N. The Path towards Sustainable Energy. *Nat. Mater.* **2017**, *16* (1), 16–22.
- (2) Zhao, X.; Shi, J.; Ji, Y.; Liu, Y. The Electronic Structure Underlying Electrocatalysis of Two-dimensional Materials. *Wiley Interdiscip. Rev.: Comput. Mol. Sci.* **2019**, *9* (6), No. e1418.
- (3) Ma, R.; Lin, G.; Zhou, Y.; Liu, Q.; Zhang, T.; Shan, G.; Yang, M.; Wang, J. A Review of Oxygen Reduction Mechanisms for Metal-Free Carbon-Based Electrocatalysts. *Npj Comput. Mater.* **2019**, *5* (1), 78.
- (4) Campos-Martin, J. M.; Blanco-Brieva, G.; Fierro, J. L. G. Hydrogen Peroxide Synthesis: An Outlook beyond the Anthraquinone Process. *Angew. Chem., Int. Ed.* **2006**, *45* (42), 6962–6984.
- (5) Yang, S.; Verdaguera-Casadevall, A.; Arnarson, L.; Silvioli, L.; Čolić, V.; Frydendal, R.; Rossmeisl, J.; Chorkendorff, I.; Stephens, I. E. L. Toward the Decentralized Electrochemical Production of  $H_2O_2$ : A Focus on the Catalysis. *ACS Catal.* **2018**, *8* (5), 4064–4081.
- (6) Mase, K.; Yoneda, M.; Yamada, Y.; Fukuzumi, S. Seawater Usable for Production and Consumption of Hydrogen Peroxide as a Solar Fuel. *Nat. Commun.* **2016**, *7* (1), 11470.
- (7) Sun, Y.; Silvioli, L.; Sahraie, N. R.; Ju, W.; Li, J.; Zitolo, A.; Li, S.; Bagger, A.; Arnarson, L.; Wang, X.; Moeller, T.; Bernsmeier, D.; Rossmeisl, J.; Jaouen, F.; Strasser, P. Activity–Selectivity Trends in the Electrochemical Production of Hydrogen Peroxide over Single-Site Metal–Nitrogen–Carbon Catalysts. *J. Am. Chem. Soc.* **2019**, *141* (31), 12372–12381.
- (8) Gao, J.; Yang, H. B.; Huang, X.; Hung, S.-F.; Cai, W.; Jia, C.; Miao, S.; Chen, H. M.; Yang, X.; Huang, Y.; Zhang, T.; Liu, B. Enabling Direct  $H_2O_2$  Production in Acidic Media through Rational Design of Transition Metal Single Atom Catalyst. *Chem* **2020**, *6* (3), 658–674.
- (9) Jirkovský, J. S.; Panas, I.; Ahlberg, E.; Halasa, M.; Romaní, S.; Schiffrin, D. J. Single Atom Hot-Spots at Au–Pd Nanoalloys for Electrocatalytic  $H_2O_2$  Production. *J. Am. Chem. Soc.* **2011**, *133* (48), 19432–19441.
- (10) Čolić, V.; Yang, S.; Révay, Z.; Stephens, I. E. L.; Chorkendorff, I. Carbon Catalysts for Electrochemical Hydrogen Peroxide Production in Acidic Media. *Electrochim. Acta* **2018**, *272*, 192–202.
- (11) Yamanaka, I.; Onizawa, T.; Takenaka, S.; Otsuka, K. Direct and Continuous Production of Hydrogen Peroxide with 93% Selectivity Using a Fuel-Cell System. *Angew. Chem., Int. Ed.* **2003**, *42* (31), 3653–3655.
- (12) San Roman, D.; Krishnamurthy, D.; Garg, R.; Hafiz, H.; Lamparski, M.; Nuhfer, N. T.; Meunier, V.; Viswanathan, V.; Cohen-Karni, T. Engineering Three-Dimensional (3D) Out-of-Plane Graphene Edge Sites for Highly Selective Two-Electron Oxygen Reduction Electrocatalysis. *ACS Catal.* **2020**, *10* (3), 1993–2008.
- (13) Nørskov, J. K.; Rossmeisl, J.; Logadottir, A.; Lindqvist, L.; Kitchin, J. R.; Bligaard, T.; Jónsson, H. Origin of the Overpotential for Oxygen Reduction at a Fuel-Cell Cathode. *J. Phys. Chem. B* **2004**, *108* (46), 17886–17892.
- (14) Chan, K.; Nørskov, J. K. Electrochemical Barriers Made Simple. *J. Phys. Chem. Lett.* **2015**, *6* (14), 2663–2668.
- (15) Taylor, C. D.; Wasileski, S. A.; Filhol, J.-S.; Neurock, M. First Principles Reaction Modeling of the Electrochemical Interface: Consideration and Calculation of a Tunable Surface Potential from Atomic and Electronic Structure. *Phys. Rev. B: Condens. Matter Mater. Phys.* **2006**, *73* (16), 165402.
- (16) Akhade, S. A.; Nidzyn, R. M.; Rostamikia, G.; Janik, M. J. Using Brønsted-Evans-Polanyi Relations to Predict Electrode Potential-Dependent Activation Energies. *Catal. Today* **2018**, *312*, 82–91.

- (17) Otani, M.; Sugino, O. First-Principles Calculations of Charged Surfaces and Interfaces: A Plane-Wave Nonrepeated Slab Approach. *Phys. Rev. B: Condens. Matter Mater. Phys.* **2006**, *73* (11), 115407.
- (18) Surendralal, S.; Todorova, M.; Finn, M. W.; Neugebauer, J. First-Principles Approach to Model Electrochemical Reactions: Understanding the Fundamental Mechanisms behind Mg Corrosion. *Phys. Rev. Lett.* **2018**, *120* (24), 246801.
- (19) Bonnet, N.; Morishita, T.; Sugino, O.; Otani, M. First-Principles Molecular Dynamics at a Constant Electrode Potential. *Phys. Rev. Lett.* **2012**, *109* (26), 266101.
- (20) Sundaraman, R.; Goddard, W. A., III; Arias, T. A. Grand Canonical Electronic Density-Functional Theory: Algorithms and Applications to Electrochemistry. *J. Chem. Phys.* **2017**, *146* (11), 114104.
- (21) Kastlunger, G.; Lindgren, P.; Peterson, A. A. Controlled-Potential Simulation of Elementary Electrochemical Reactions: Proton Discharge on Metal Surfaces. *J. Phys. Chem. C* **2018**, *122* (24), 12771–12781.
- (22) Hörmann, N. G.; Andreussi, O.; Marzari, N. Grand Canonical Simulations of Electrochemical Interfaces in Implicit Solvation Models. *J. Chem. Phys.* **2019**, *150* (4), 041730.
- (23) Zhao, X.; Liu, Y. Unveiling the Active Structure of Single Nickel Atom Catalysis: Critical Roles of Charge Capacity and Hydrogen Bonding. *J. Am. Chem. Soc.* **2020**, *142* (12), 5773–5777.
- (24) Kim, D.; Shi, J.; Liu, Y. Substantial Impact of Charge on Electrochemical Reactions of Two-Dimensional Materials. *J. Am. Chem. Soc.* **2018**, *140* (29), 9127–9131.
- (25) Nong, H. N.; Falling, L. J.; Bergmann, A.; Klingenhof, M.; Tran, H. P.; Spöri, C.; Mom, R.; Timoshenko, J.; Zichittella, G.; Knop-Gericke, A.; Piccinin, S.; Pérez-Ramírez, J.; Cuenya, B. R.; Schlägl, R.; Strasser, P.; Teschner, D.; Jones, T. E. Key Role of Chemistry versus Bias in Electrocatalytic Oxygen Evolution. *Nature* **2020**, *587* (7834), 408–413.
- (26) Viswanathan, V.; Hansen, H. A.; Rossmeisl, J.; Nørskov, J. K. Unifying the 2e- and 4e- Reduction of Oxygen on Metal Surfaces. *J. Phys. Chem. Lett.* **2012**, *3* (20), 2948–2951.
- (27) Ju, W.; Bagger, A.; Hao, G.-P.; Varela, A. S.; Sinev, I.; Bon, V.; Cuenya, B. R.; Kaskel, S.; Rossmeisl, J.; Strasser, P. Understanding Activity and Selectivity of Metal-Nitrogen-Doped Carbon Catalysts for Electrochemical Reduction of CO<sub>2</sub>. *Nat. Commun.* **2017**, *8* (1), 944.
- (28) Ling, C.; Zhang, Y.; Li, Q.; Bai, X.; Shi, L.; Wang, J. New Mechanism for N<sub>2</sub> Reduction: The Essential Role of Surface Hydrogenation. *J. Am. Chem. Soc.* **2019**, *141* (45), 18264–18270.
- (29) Gauthier, J. A.; Dickens, C. F.; Heenen, H. H.; Vijay, S.; Ringe, S.; Chan, K. Unified Approach to Implicit and Explicit Solvent Simulations of Electrochemical Reaction Energetics. *J. Chem. Theory Comput.* **2019**, *15* (12), 6895–6906.
- (30) Lindgren, P.; Kastlunger, G.; Peterson, A. A. A Challenge to the G ~ 0 Interpretation of Hydrogen Evolution. *ACS Catal.* **2020**, *10*, 121–128.
- (31) Sheng, T.; Sun, S.-G. Free Energy Landscape of Electrocatalytic CO<sub>2</sub> Reduction to CO on Aqueous FeN<sub>4</sub> Center Embedded Graphene Studied by Ab Initio Molecular Dynamics Simulations. *Chem. Phys. Lett.* **2017**, *688*, 37–42.
- (32) Cheng, T.; Xiao, H.; Goddard, W. A. Free-Energy Barriers and Reaction Mechanisms for the Electrochemical Reduction of CO on the Cu(100) Surface, Including Multiple Layers of Explicit Solvent at PH 0. *J. Phys. Chem. Lett.* **2015**, *6* (23), 4767–4773.
- (33) Cheng, T.; Xiao, H.; Goddard, W. A. Reaction Mechanisms for the Electrochemical Reduction of CO<sub>2</sub> to CO and Formate on the Cu(100) Surface at 298K from Quantum Mechanics Free Energy Calculations with Explicit Water. *J. Am. Chem. Soc.* **2016**, *138*, 13802.
- (34) Mathew, K.; Kolluru, V. S. C.; Mula, S.; Steinmann, S. N.; Hennig, R. G. Implicit Self-Consistent Electrolyte Model in Plane-Wave Density-Functional Theory. *J. Chem. Phys.* **2019**, *151* (23), 234101.
- (35) Mathew, K.; Sundaraman, R.; Letchworth-Weaver, K.; Arias, T. A.; Hennig, R. G. Implicit Solvation Model for Density-Functional Study of Nanocrystal Surfaces and Reaction Pathways. *J. Chem. Phys.* **2014**, *140* (8), 084106.
- (36) Woo, T. K.; Margl, P. M.; Blöchl, P. E.; Ziegler, T. A Combined Car–Parrinello QM/MM Implementation for Ab Initio Molecular Dynamics Simulations of Extended Systems: Application to Transition Metal Catalysis. *J. Phys. Chem. B* **1997**, *101* (40), 7877–7880.
- (37) Jarzynski, C. Nonequilibrium Equality for Free Energy Differences. *Phys. Rev. Lett.* **1997**, *78* (14), 2690–2693.
- (38) Sprik, M.; Ciccotti, G. Free Energy from Constrained Molecular Dynamics. *J. Chem. Phys.* **1998**, *109* (18), 7737–7744.
- (39) Gao, G.; Wang, L.-W. Substantial Potential Effects on Single-Atom Catalysts for the Oxygen Evolution Reaction Simulated via a Fixed-Potential Method. *J. Catal.* **2020**, *391*, 530–538.
- (40) McCaffrey, D. L.; Nguyen, S. C.; Cox, S. J.; Weller, H.; Alivisatos, A. P.; Geissler, P. L.; Saykally, R. J. Mechanism of Ion Adsorption to Aqueous Interfaces: Graphene/Water vs. Air/Water. *Proc. Natl. Acad. Sci. U. S. A.* **2017**, *114* (51), 13369–13373.